ADVANCED MATERIALS INTERFACES

www.advmatinterfaces.de

Lithium-Metal Foil Surface Modification: An Effective Method to Improve the Cycling Performance of Lithium-Metal Batteries

Jens Becking, Albert Gröbmeyer, Martin Kolek, Uta Rodehorst, Susanne Schulze, Martin Winter, Peter Bieker, and Marian Cristian Stan*

Lithium metal as an electrode material possesses a native surface film, which leads to a rough surface and this has a negative impact on the cycling behavior. A simple, fast, and reproducible technique is shown, which makes it possible to flatten and thin the native surface film of the lithium-metal anode. Atomic force microscopy and scanning electron microscopy images are presented to verify the success of the method and X-ray photoelectron spectroscopy measurements reveal that the chemical composition of the lithium surface is also changed. Furthermore, galvanostatic measurements indicate superior cycling behavior of the surface modified electrodes compared to the as-received ones. These results demonstrate that the native surface film plays a key role in the application of lithium metal as an anode material for lithium-metal batteries and that the shown surface modification method is an excellent tool to obtain better performing Li metal electrodes.

1. Introduction

The rechargeable lithium-ion battery (LIB) enjoys big commercial success in the portable consumer electronics market and is presently expending to the automotive and industrial sector.[1] The commercial success was only possible after the lithium-metal anode had been replaced by an insertion or intercalation reaction based anode that in most cases is still made out of carbon, in particular graphite.[2–6]

With the emergence of new application markets demanding a higher energy density, battery systems with cathode active materials being oxygen,[7] sulfur, or fluoride and with lithium metal as the anode material are reconsidered as viable options.[8–12] Although the lithium-metal anode has the advantages of both high gravimetric and volumetric capacities (3862 Ah kg^{-1} and 2085 Ah L^{-1})[13] and is already successfully used in primary batteries, it is still plagued by a series of issues that limit its successful operation in rechargeable applications, when organic solvent based electrolytes are used.[14] One of them is the nature of the lithium-metal dissolution and redeposition in the discharge and charge process together with the composition of the solid electrolyte interphase (SEI)[15,16] that is formed immediately after electrolyte addition and continues to form, grow and alter during cycling,[17] which limits the rechargeability in these battery systems and decreases their safety.[15,18,19] The SEI, though not being a homogeneous single phase, varies in composition and thickness and these differences lead to inhomogeneous and thus locally different current densities during the discharge and charge process, which can ultimately cause the formation of high surface area lithium (HSAL) during lithium deposition (charging) and hole/pit formation during dissolution (discharging).[20–22] In the worst case, the HSAL morphology takes the form of dendrites, i.e., small needle like lithium deposits that can grow through the separator from the anode towards the cathode. This process can lead to an internal short circuit of the cell resulting in local overheating and possibly cause a cell fire due to an increased reactivity with the electrolyte and the low melting point of lithium (180.54 °C).[23]

Practical approaches to improve the rechargeable lithium-metal anode from the electrode material's point of view concentrate on either using coated lithium powder[24,25] or foil[26] and lithium with surface micropatterning.[27,28] The main underlying principle is increasing the specific surface area thus decreasing the effective current density and the resulting overpotential. However, the behavior of the lithium-metal electrode is quite complex and electrolyte-dependent[22,29–31] and there is a need to identify the optimal conditions under which lithium-metal electrodes can cycle with both an increased reversibility and low overpotentials.[32] As-received lithium-metal foil contains several contaminants,[33] particularly on the surface.[34] In addition, even a new lithium foil

J. Becking, A. Gröbmeyer, M. Kolek, Dr. U. Rodehorst, Dr. S. Schulze, Prof. M. Winter, Dr. P. Bieker, Dr. M. C. Stan
MEET Battery Research Center
Institute of Physical Chemistry
University of Muenster
Corrensstrasse 46, 48149 Muenster, Germany
E-mail: peter.bieker@uni-muenster.de

Prof. M. Winter
Helmholtz-Institute Muenster (HI MS), IEK-12
Forschungszentrum Juelich GmbH
Corrensstrasse 46, 48149 Muenster, Germany

DOI: 10.1002/admi.201700166

that is considered to be smooth shows a non-negligible surface roughness that inevitably affects the deposition morphology.[35] As known from science of metallurgy, the shape of the (over-)potential profiles is mainly influenced by the change in the electrode surface and can therefore be equal to the crystallization overpotential.[36] This approach can also be applied to lithium-metal anodes as former studies on lithium polymer batteries have shown.[37]

In this study, the effect of both, the native surface film as well as the initial surface roughness on the electrochemical performance of lithium-metal anodes was investigated. We observed that during the initial cycles these parameters were crucial. Nevertheless, the beneficial effect of the initial surface chemical composition and morphology were gradually lost, due to the repeated deposition of fresh lithium and its irreversible reaction with the electrolyte with increasing dissolution–deposition cycle number. At this time, it is also important to mention that lithium-metal electrodes are usually used as received as auxiliary electrodes in half-cell configuration. In our study, we observed, that the surface's initial roughness (in particular the surface defects) is critical for the initial lithium deposition morphology and that the resistivity of the native surface film has an influence on both the cycling performance and the overpotentials of the deposition and dissolution processes. Furthermore, the method to minimize the contribution of both the native surface film and the surface roughness described here, is simple, fast, and reproducible.

2. Results and Discussion

The surface morphology of the as-received lithium foil was first characterized by scanning electron microscopy (SEM) (**Figure 1**a,b). The images indicate a very rough surface with scratches and splines while at a higher magnification (Figure 1b), a multitude of surface defects are noticeable.

The Atomic force microscopy (AFM) image showing the 3D surface topology measured in the AC mode of the as-received lithium foil (Figure 1c) agrees well with the SEM observations made. The average roughness (R_a) and the maximum profile height of the mountain- and valley-like structures is 130 ± 10 nm and 1.37 ± 0.01 µm, respectively. The R_a value is obtained as the average of all points along the length of the evaluation line in the middle of the AFM image (Figure 1c). These mountain-like structures with deep valleys on the surface of the as-received lithium foil can act as preferential "hot spots" for the lithium dissolution and deposition. Furthermore, the surface of the as-received lithium foil is always covered by a native film, resulting from the reaction of the fresh lithium metal with atmospheric contaminants during the fabrication process.[33,37] The surface chemistry of the native surface film is highly dependent on the atmospheric conditions in which the lithium foils are prepared. In the X-ray photoelectron spectroscopy (XPS) spectra (Figure S1a, Supporting Information) measured for the as-received lithium foil for the C 1s region four peaks are identified. The main peak present at 289.9(5) eV is attributed to the presence of Li_2CO_3 at the surface of the as-received lithium foil originating from the gas treatment during the fabrication process.[38] The peak at 288.4(5) eV is ascribed to the C—O group in COOR followed by a peak at 286.4(5) eV assigned to the C—C—O group. The peak at 284.6(5) eV is attributed to the C—H group originating from the presence of the adventitious hydrocarbon in the XPS chamber. Additionally, the

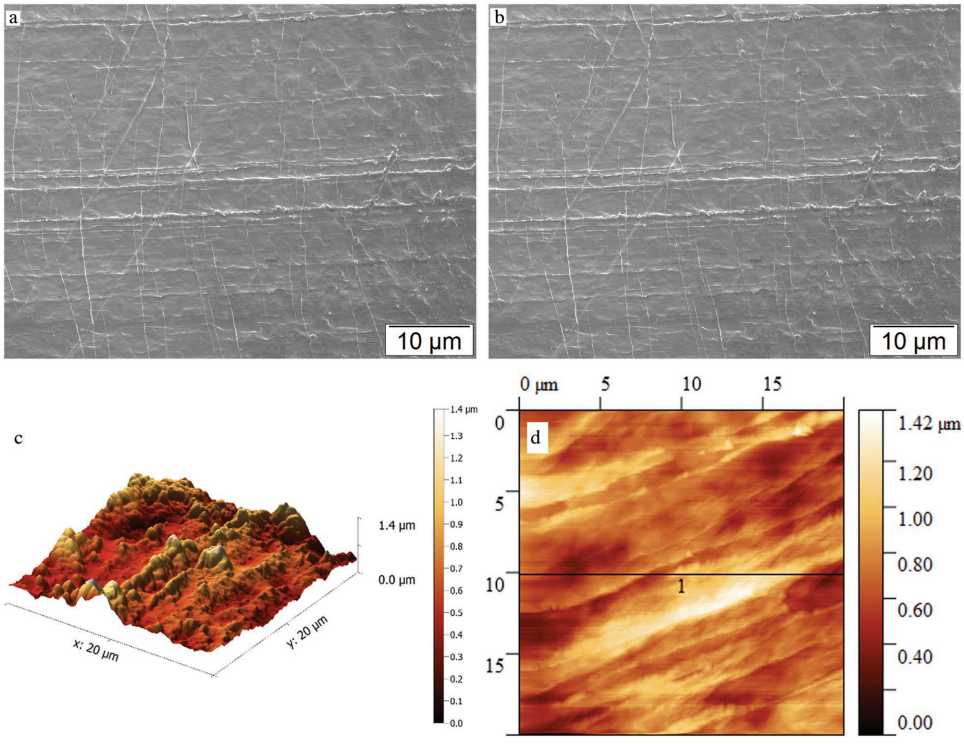

Figure 1. SEM images of the as-received lithium foil taken with a magnification of a) 50× and b) 1000×, and c) the AFM surface topology 3D image as well as d) 2D image of the as-received lithium foil.

presence of Li_2CO_3 on the surface of the as-received lithium foil is further confirmed by the presence of the peaks at 532.2(5) eV in the O 1s spectra (Figure S1b, Supporting Information) and at 55.4(5) eV in the Li 1s spectra (Figure S1c, Supporting Information). LiOH, however, identified in the O 1s spectrum can result from the contamination with atmospheric moisture during the lithium sample transfer to the XPS chamber. These results indicate that the surface composition of the as-received lithium foil mainly consists of Li_2CO_3. The presence of the native surface film on the lithium foil can also have an effect on the electrochemical performance of the lithium-metal anodes, and is particularly detrimental during the cell production process in situations, when surface film control, e.g., by design of an artificial protective film is desired for protective coverage of the lithium-metal surface.[39]

Only a few articles are available describing methods for the removal of the native surface film on lithium metal and of these an even smaller number are carried out with reproducible results and can be scaled up. Among these methods, removal of the native surface film by scrapping it off with a sharp blade is the most common,[39–41] while other methods involving the washing and polishing of the lithium foil in hydrocarbons are also frequently mentioned.[42,43] In this work, a simple, fast, cheap, and solvent-free technique without the production of any unwanted lithium waste is applied to smoothen the surface of the as-received lithium foil and at the same time to effectively thin the native surface film. This technique is based on applying a uniaxial pressure on the as-received lithium foil (500 µm) using a tabletop roll-press and stepwise decreasing of the distance between the two rolls. In this way, the thickness of the lithium foil is reduced until a predefined value (here: 350 µm) is achieved. Such a decrease in thickness also results in a smoothening of surface defects and imperfections as those observed in Figure 1. In **Figure 2**, the SEM and AFM images of the lithium foil after the roll-press process are presented. After applying the roll-press technique only a few splines remain (Figure 2b) while a striking difference is observable in the AFM images presenting the topography of the roll-pressed (Figure 2c) and as-received lithium foil (Figure 1d). This is further verified by the height profiles in Figure 2d. Fewer mountain-like structures and deep valleys are identified, although some valleys still remain as a result of the significant imperfections in the carrier material, i.e., siliconized Mylar foil (AFM images of the carrier material are given for comparison in Figure S2, Supporting Information).

The height profile of the roll-pressed lithium foil and the R_a value indicate that the roll-press technique decreases the surface roughness of the as-received lithium foil. The R_a value of the former that is 37.3 nm represents 1/3 of the R_a value of the latter with a maximum vertical spacing of the real surface from its ideal form (maximum roughness height) of 0.35 µm. The chemical composition of the roll-pressed lithium foil was investigated by means of XPS measurements and the results are provided in Figure S1d–f (Supporting Information). Although the chemical composition of the lithium surfaces in both samples is identical, the main differences are in the intensities of the components that are covering these surfaces. In the C 1s spectra as well as in the O 1s spectra the most striking differences are observed. In the C 1s spectra, for the as-received lithium foil (Figure S1a, Supporting Information) and

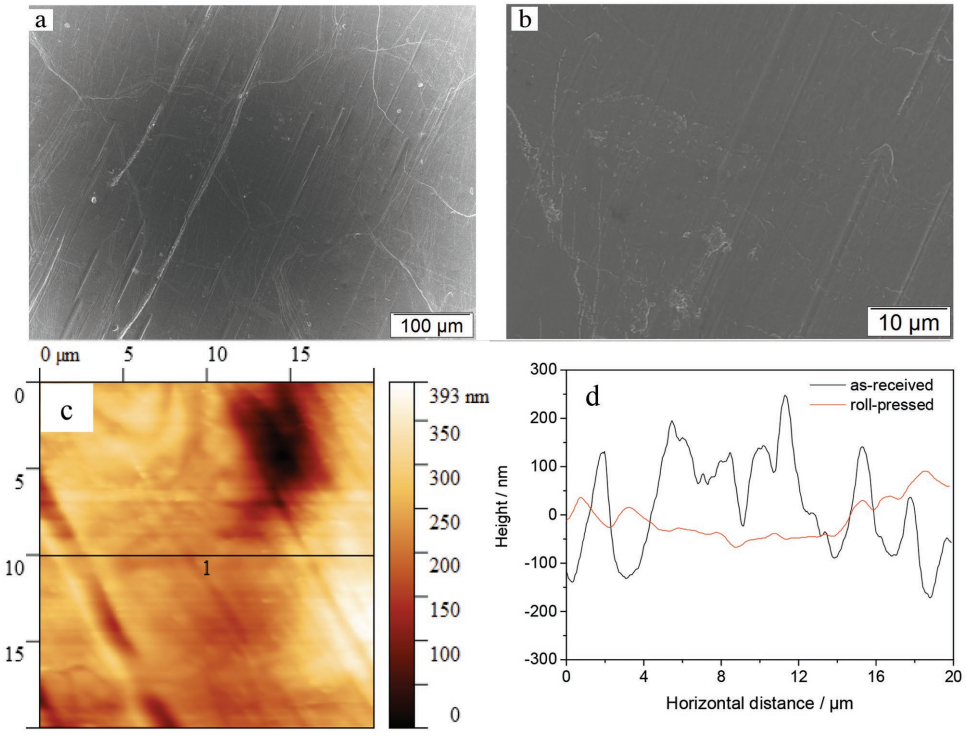

Figure 2. SEM images of roll-press lithium foil taken with a magnification of a) 50×, b) 1000×, and the corresponding c) AFM surface topology of the roll-pressed lithium foil and d) the height profiles taken from AFM results of the two samples.

roll-press lithium foil (Figure S1d, Supporting Information), the change of the Li_2CO_3 peak intensity at 289.8(5) eV from 17.7 to only 2.9 at% implies a change in the concentration of the Li_2CO_3 layer on the surface of the lithium foil. This observation is further confirmed by the intensity reduction of the Li_2O component in the O 1s spectra on the surface of the two samples. The reduction in the at% of both Li_2CO_3 and Li_2O peaks indicates that the thickness of the native film is reduced as a result of the lithium foil thinning during the roll-press process. Combining these results with the observations in Figure 2, it can be concluded that the roll-press technique applied to the as-received lithium foil, reduces the roughness of the electrodes' surfaces and at the same time thins the native surface film. Such a thinning occurs during the stepwise decrease of the roll-press gauge along the *z*-axis, when due to its soft nature the lithium foil (Young's modulus 4.9 GPa) expands in both the *x*- and *y*-direction. Although the chemical composition of the native film on both samples is identical as pointed out by the XPS measurements in Figures S1 and S3 in the Supporting Information (but with different concentrations), the XPS depth profiling measurements (Figure S3, Supporting Information) imply, based on the decrease of the carbon concentration, that the native surface film on the roll-press lithium is thinner than that on the as-received lithium foil. The presence of Si 2p peak in the XPS spectra of the roll-pressed lithium foil is due to the fact that the roll-press process has been carried out by placing the as-received lithium foil between two siliconized Mylar foils, as described in the Experimental Section.

To assess the importance of the surface treatment for the electrochemical performance of the lithium-metal anodes, the cycling behavior and the SEI impedance evolution of these electrodes was carried out and the results are presented in **Figure 3**. The mechanism of the lithium dissolution–deposition process during constant current charge–discharge measurements with a specific current of 0.1 mA cm^{-2} for 50 cycles is characterized by observing the evolution of the lithium overvoltage. Its values for the as-received lithium-metal anodes are higher and unsteady during the complete process of the lithium dissolution–deposition (Figure 3a). However, low and stable overvoltages are observed with the roll-pressed lithium-metal anodes during both the dissolution as well as the deposition process (Figure 3b). The SEI impedance evolution of the lithium-metal anodes with the native surface film and with the thinned native surface film is investigated by electrochemical impedance spectroscopy (EIS) during the lithium dissolution–deposition process. In Figure 3c,d the Nyquist plots are recorded under open circuit voltage (OCV) conditions in the initial state and after the 10th, 20th, 30th, 40th, and 50th cycle. Comparing

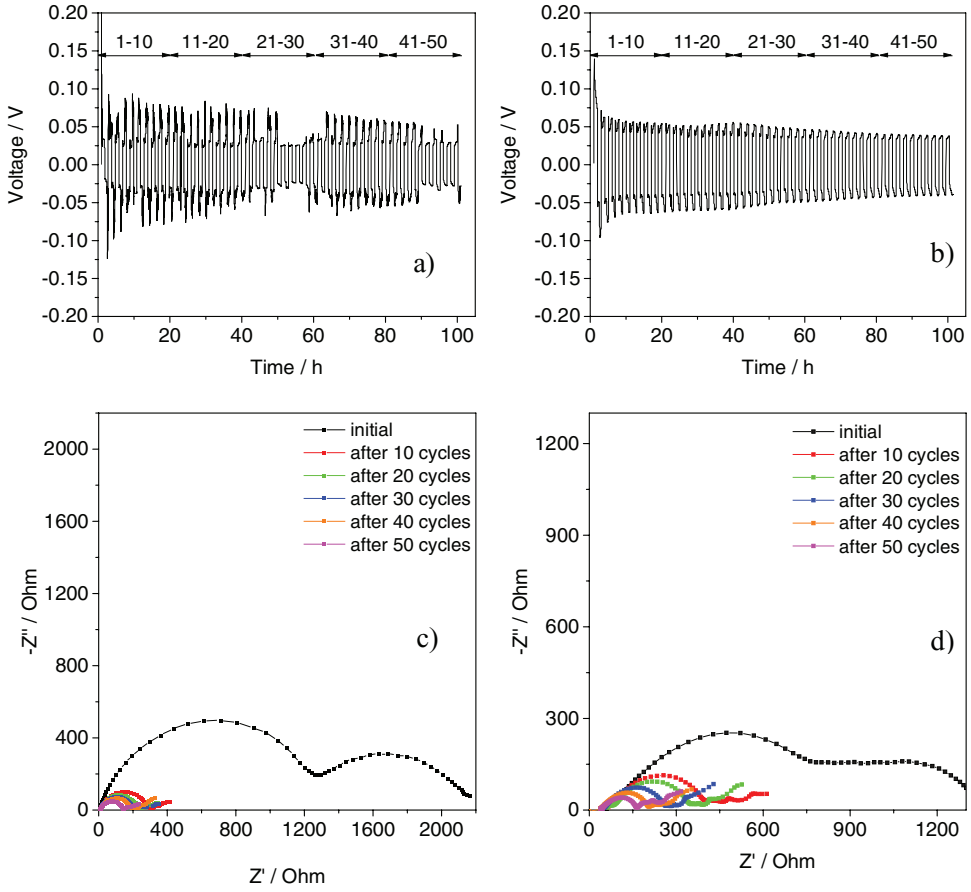

Figure 3. Evolution of the voltage and the Nyquist plot of the lithium dissolution–deposition process a,c) for as-received lithium and b,d) with roll-pressed lithium-metal anodes cycled in CR 2032 symmetrical lithium cells at a current density of 0.1 mA cm^{-2} in 1 M LiTFSI in TEGDME:DIOX 1:1 (by volume) as electrolyte.

the initial impedances of the two electrodes (Figure 3c,d), a higher impedance is shown by the CR 2032 cell assembled with the as-received lithium-metal anode. This difference represents a clear proof that the surface of the lithium-metal electrode modified by the roll-press method has an effect on the electrochemical behavior of the lithium-metal anodes. Later in this paper, the meaning of the overpotential evolution during continuous cycling will be discussed in more detail.

The continuous dissolution–deposition of the lithium of both electrodes also results in a decrease of the cell impedance. Even though at the beginning of the cycling, a clear difference between the cell impedance of the two cells is observed, after only 10 cycles this difference is negligible. An explanation for the observed behavior is that the native surface film on the lithium-metal electrodes dominates the initial cell impedance, while with an increasing number of the dissolution–deposition cycles the changes of the electrode surface morphology and the creation of fresh lithium surfaces on both electrodes become more relevant. The semicircles from the Nyquist plots in Figure 3c,d are fitted using the *R–C* equivalent electric circuit presented in the inset of **Figure 4**. The fitting is carried out using a constant phase element (CPE) instead of an ideal capacitor due to the depressed semicircles observed in the Nyquist plots. The reasons for such nonideal behavior are related to the roughness of the electrode–electrolyte interface, inhomogeneous grain boundary distribution or due to ion dynamics.[44] In these plots, the decrease of the resistance (R_{SEI}) with time is attributed to the change in the interphase between the lithium-metal electrode and the electrolyte.

The initial R_{SEI} of the roll-pressed lithium-metal anode decreases with increasing cycle number from 852 to 124 Ω after 50 cycles. In contrast, the R_{SEI} of the as-received lithium-metal anode after 50 cycles shows a value of 150 Ω. Thus, we can conclude that the roll-press technique reduces the thickness of the native surface film and that the resistance of the lithium electrode after 50 cycles is a combined resistance including both the contribution from the native surface film and from the SEI that is formed during cycling (formation of fresh lithium-metal surfaces). Previously, it was shown that

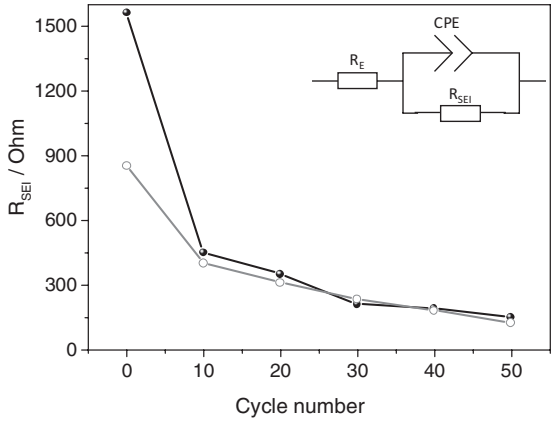

Figure 4. Evolution of the R_{SEI} of as-received (black) and roll-pressed (red) lithium-metal anodes during the first 50 cycles of lithium dissolution–deposition at a current density of 0.1 mA cm^{-2}. Inset: The equivalent electrical circuit used to fit the complex Nyquist plot.

the overvoltage during the dissolution–deposition process is affected by the lithium-metal anode surface roughness.[22,24] However, the evolution of the R_{SEI} within a cell with increasing cycling number, presented in Figure 4, indicates, that the initial resistance of the lithium-metal anode due to the presence of the native surface film also influences, how the SEI is formed, when the fresh lithium surface is in contact with the electrolyte, i.e., 1 M lithium bis(trifluoromethanesulfonyl)imide (LiTFSI) in tetraethylene glycol dimethyl ether (TEGDME) and 1,3-dioxolane (DIOX) 1:1 (by volume). The type and mechanism of the SEI formation play a crucial role for the electrochemical performance of the lithium-metal anodes. Additionally, the cycling experiments in symmetrical three electrode Swagelok cells with lithium metal as the working electrode were carried out for more than 900 cycles using a constant current of 0.113 mA. The evolution of the overpotentials of the lithium dissolution–deposition process within the first 900 cycles is given in **Figure 5**.

During cycling, the overpotentials of the dissolution–deposition process for the two lithium-metal anodes decreases, indicating that there is a change in both the surface morphology and composition (Figure 5a,b). As previously discussed in Figure 4, the breaking of the native film due to the continuous lithium dissolution and deposition process leads to a decrease of the R_{SEI} and thus a decrease in the overpotentials due to the formation of fresh lithium surfaces.[45] For the as-received lithium-metal anode, the first dissolution process occurs at 85 mV versus Li/Li$^+$ while for the reverse direction the deposition potential starts from −48 mV versus Li/Li$^+$. However, after almost 70 cycles both processes show a potential plateau that reaches a value of 17 mV versus Li/Li$^+$ and −17 mV versus Li/Li$^+$, respectively (Figure 5c). A similar behavior is observed for the roll-pressed lithium-metal anode with the only striking difference being in the initial cycles of the lithium dissolution–deposition process. In this case the overpotentials are reduced due to a change of the native surface film. The lower overpotentials values can give also an indication of the lithium deposits morphology as has been previously reported,[45] however the changes observed here are mainly related to the initial native surface film resistance as it will be discussed in the following. During the first cycle for the roll-pressed lithium-metal anode, the overpotentials of the dissolution–deposition process occur at 40 mV and −39 mV versus Li/Li$^+$, respectively (Figure 5d). Compared to the previous experiment, after 70 continuous cycles, the overpotentials stabilize for the rest of the cycling process at a maximum of 20 and −20 mV versus Li/Li$^+$ for the dissolution and deposition process, respectively. These values of the overpotentials are similar for the two lithium-metal anodes due to the continuous dissolution and redeposition of the lithium and also the surface roughness due to the formation of HSAL.

The morphology and the chemistry of both lithium-metal anodes, for the as-received and roll-pressed lithium foil, are investigated after the deposition process of the 1st, 5th, 10th, and 15th cycle by SEM and XPS. The SEM images of the cycled lithium-metal anodes with the as-received lithium foil and the roll-pressed lithium foil are presented in **Figure 6**.

The observed potential differences, between the lithium-metal anode used as received (Figure 5c) and the one with the

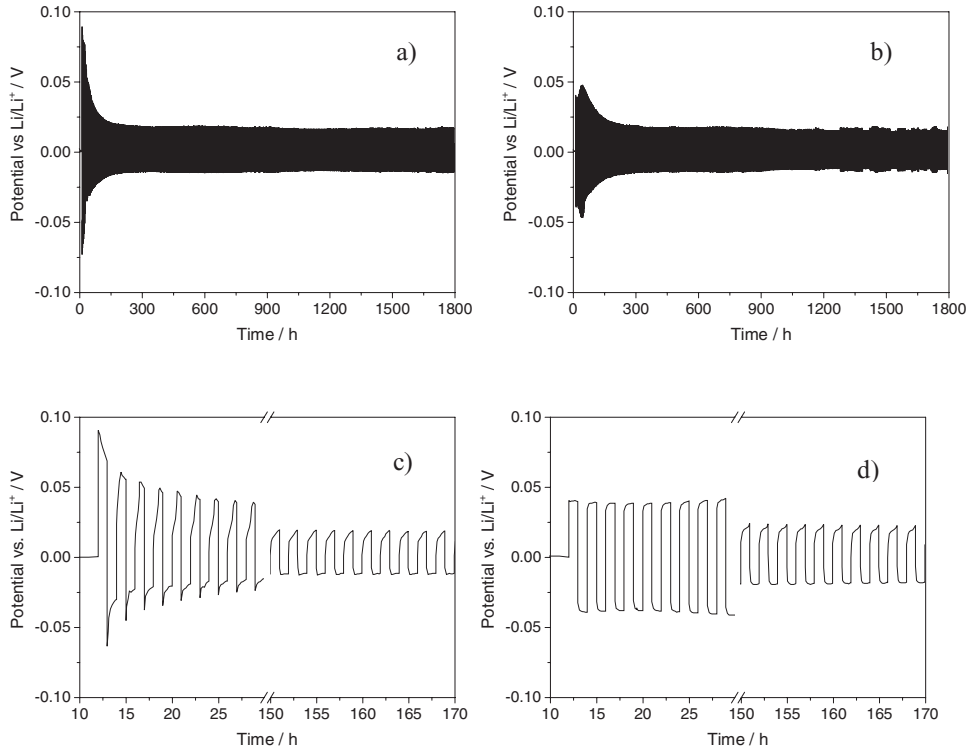

Figure 5. Evolution of the potentials of symmetrical lithium cells assembled with a,c) as-received lithium and b,d) roll-pressed lithium-metal anodes using a current density of 0.1 mA cm^{-2} in 1 M LiTFSI in TEGDME:DIOX 1:1 (by volume). A magnified view of the corresponding lithium foils for the first 1–9 cycles and intermediate 70–80 cycles is presented c,d).

roll-press treatment (Figure 5d), in the earlier stages of the lithium dissolution–deposition process are also reflected by the morphology differences. During the first cycle, the potential of the dissolution process of the lithium-metal anode used as received starts at 88 mV versus Li/Li^+, while in the case of the roll-pressed lithium-metal anode the potential decreases to 44 mV versus Li/Li^+. Such behavior represents a clear indication that both the current density[22] and the initial surface chemistry play an important role in the lithium dissolution process of the lithium-metal electrodes as shown by the XPS (Figure S1, Supporting Information) and EIS (Figure 3) investigations.

Comparing the SEM images of the as-received lithium-metal anode (Figure 6a) with those of the roll-pressed one after 5 cycles (Figure 6d) the advantages of the native surface film thinning by means of the roll-press method are clearly evident. In the case of the as-received lithium-metal anode, the lithium dissolution–deposition process occurs predominantly at prominent sites, i.e., at the mountain- and valley-like regions while a more homogeneous lithium dissolution–deposition is observed for the lithium foil where these structures were reduced (equivalent to the thinning of the native surface film). The inhomogeneity of the lithium dissolution–deposition process for the as-received sample (Figure 6a) is further proven by sections showing no or little lithium dissolution–deposition and the regions, where these processes are favored resulting in lithium deposits with morphologies resembling leaf-veins. However, even after mechanical treatment, it is not possible to completely remove the mountain- and valley-like structures that promote the formation of HSAL with leaf-vein structures, although the thickness of the as-received lithium electrode was reduced by 30% by the roll-press method. This is shown in Figure 6b where it is observed that the lithium dissolution–deposition for the as-received lithium foil continues to occur at the previously active regions. For the roll-pressed lithium foil, the lithium dissolution–deposition occurs in a more homogenous manner. After only 15 cycles, the surface of both lithium-metal anodes show no differences because they are fully covered by deposited HSAL (Figure 6c,f). The evolution of the HSAL formation for the two electrodes plays an important role for the performance of the lithium-metal electrodes with increasing cycling number since the time the HSAL needs to reach the separator in an inhomogeneous process is shorter than in a homogeneous process. Based on these observations, we can propose a mechanism for the lithium dissolution–deposition on the two lithium-metal anodes, which is schematically shown in **Figure 7**.

Further proof for this can be found in the XPS results of the F1s peak after the 5th, 10th, and 15th cycle (Figures S6–S11, Supporting Information), which are given in **Table 1**. The first peak at 688.8 eV is assigned to LiTFSI and a second peak at 684.9 eV is attributed to LiF. The difference between as-received and roll-pressed lithium foil is most evident after the 5th dissolution–deposition cycle. At this point, the SEI of the as-received lithium foil mainly consists of degradation products of the LiTFSI salt, that account for 82.0% while only a small amount of LiF (18.0%) is visible. The SEI of roll-press lithium-metal anode also consists mainly of LiTFSI degradation products

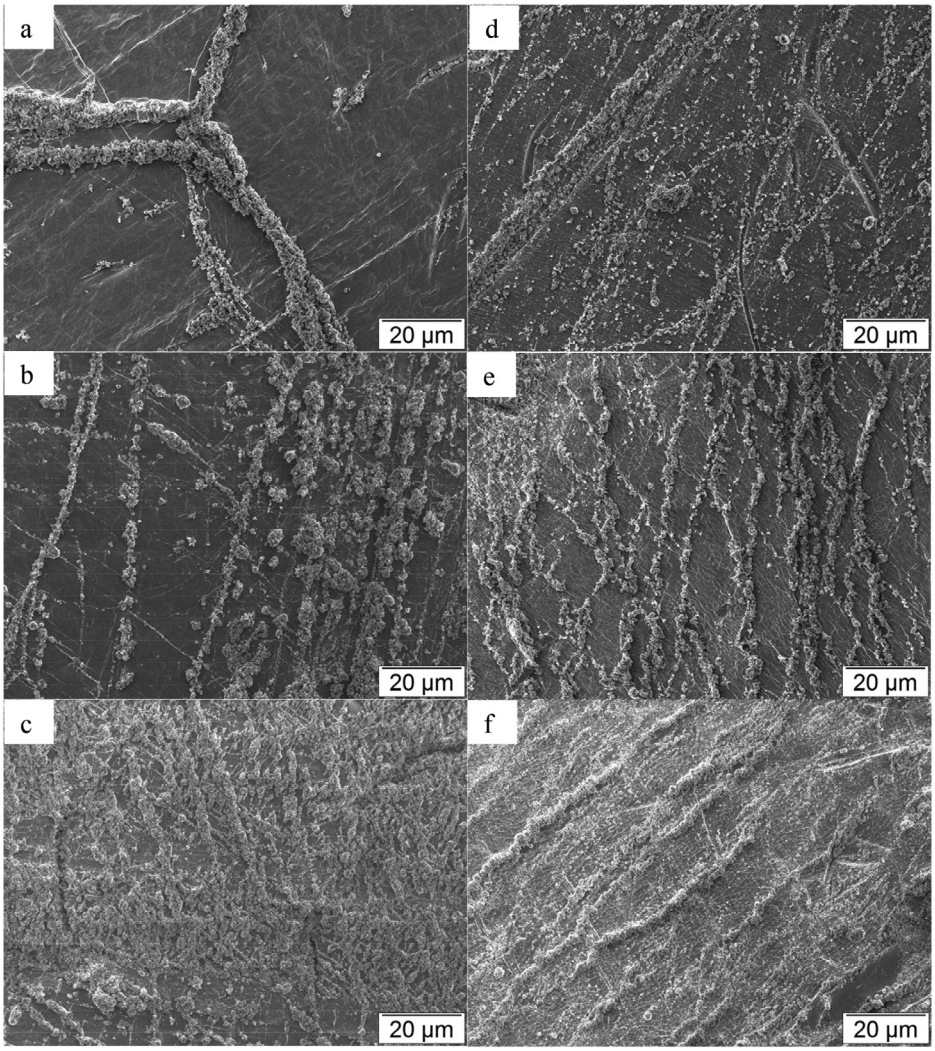

Figure 6. SEM images at a magnification of 1000× of the lithium-metal anodes after a,d) 5, b,e) 10, and c,f) 15 cycles with the as-received lithium foil a–c) and the roll-pressed foil d–f) cycled at 0.1 mA cm^{-2} in 1 M LiTFSI in TEGDME:DIOX 1:1 (by volume).

(64.5%), but the amount of LiF is two times higher than for the untreated one (35.5%). This is in line with some recent publications where they proof that an increased amount of LiF lead to reduced impedance and extended cell lifetime.[31,46,47] The ratio of LiTFSI:LiF changes for both samples from 2:1 after the 10th cycle to 1:1 after the 15th cycle. Similar to the constant current measurements the difference between the two samples is only visible during the first cycle.

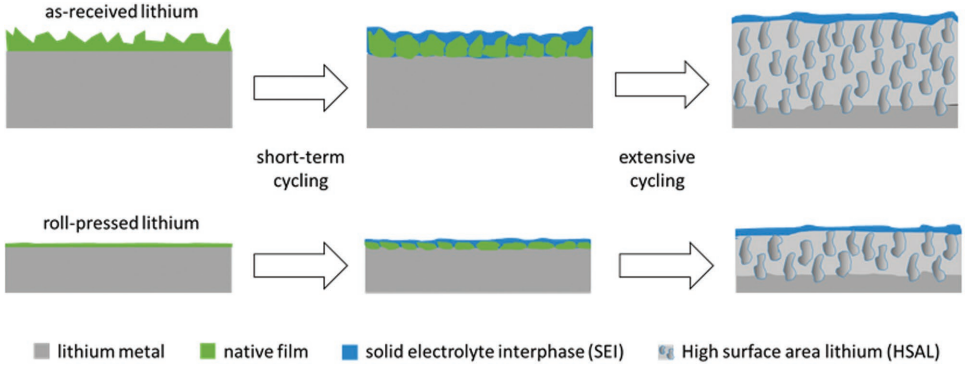

Figure 7. Schematic illustration of the behavior of the native surface film on lithium-metal anode before, after short-term and after extensive cycling.

Table 1. Binding energies (BE) and atomic percentages (at%) from XPS F 1s peak of lithium-metal anodes after 5, 10, and 15 cycles of dissolution–deposition at 0.1 mA cm^{-2}.

		As-received		Roll-pressed	
		BE [eV]	at%	BE [eV]	at%
5 cycles	LiF	684.8	18.0	684.8	35.5
	LiTFSI	688.7	82.0	688.8	64.5
10 cycles	LiF	684.9	43.9	684.9	38.2
	LiTFSI	688.8	56.1	688.7	61.8
15 cycles	LiF	684.9	55.2	684.8	49.7
	LiTFSI	688.8	44.8	688.7	50.3

3. Conclusion

In this work, the electrochemical performance of the lithium-metal electrodes was improved by applying the roll-press technique that removes the surface roughness and thins the native surface film present on the as-received lithium foil. As confirmed by AFM, SEM, and XPS the lithium surface after the roll-press treatment shows a flatter topography with fewer mountain-like structures and with a decreased concentration of the Li_2CO_3 species. Such changes in the morphology and chemical composition of the roll-pressed lithium foil surface affect the evolution of the R_{SEI} during storage as shown by the impedance measurements of symmetric lithium cells carried out at OCV. A low R_{SEI} has a positive impact on the overpotentials for the lithium dissolution–deposition process as during the first cycle, the overpotential of the dissolution process for the roll-pressed lithium-metal anode occurs 45 mV lower than for the as-received lithium foil. Comparing the values of the lithium overpotentials for the deposition process, a 9 mV lower overpotential is measured for the roll-pressed lithium foil. Furthermore, in the first 5 to 10 cycles of the dissolution–deposition process, SEM investigations confirmed homogeneous HSAL deposition for the roll-pressed lithium foil. Even though extensive cycling reduces the effect of such surface treatment, the roll-press technique can be applied to modify the surface of the lithium-metal anodes and therefore to "tailor" the electrochemical performance. This technique can also be used prior to the application of a lithium protection layer, an approach often considered for lithium-metal anodes with applications in next generation battery systems. Due to its simplicity and high effectiveness, the roll-press technique of the lithium-metal anodes represents an inexpensive method that can easily be adapted in the lithium-metal battery production process thus bringing such technologies a step closer to their commercialization.

4. Experimental Section

Preparation of Roll-Pressed Lithium-Metal Anodes: Lithium foil (Rockwood Lithium, 500 µm thickness) was rolled between two siliconized polyester foils (Mylar, PPI Adhesive Products Ltd., 100 µm thickness) in 50 µm decrements using a tabletop roll press (Hohsen Corp., HSAM-615H) to a final thickness of 350 µm.

X-Ray Photoelectron Spectroscopy: XPS measurements were carried out at a 0° angle of emission and a pass energy of 20 eV using a monochromatic Al Kα source (E_{photon} = 1486.6 eV) with a 10 mA filament current and a filament voltage source of 12 kV. The analyzed area was ≈300 µm × 700 µm. In order to compensate for the charging of the sample, a charge neutralizer was used. The C 1s peak at 284.6 eV was taken as an internal reference for the adjustment of the energy scale in the spectra. The XPS samples were delivered in sealed vials that enable the transfer without the sample having any contact with oxygen and moisture from the atmosphere. Afterward the sealed vials were opened in a mini glovebox connected to the XPS device. The fitting was carried out with CasaXPS.

Dissolution/Deposition: Three electrode Swagelok cells and two electrode CR 2032 coin cells were prepared in a dry room (0.02% moisture content). Dissolution/deposition experiments were performed at 20 °C using a MACCOR battery cycler (MACCOR Series 4000) for long-term experiments while a VMP3 (Bio-Logic) was used for short-term experiments. As-received or roll-press lithium foil was used as counter and working electrode, respectively. For 100 cycles a current of 0.113 mA (0.1 mA cm^{-2}) was applied to the 12 mm diameter electrodes. Each cycle consisted of a 1 h dissolution step and 1 h deposition step. As the electrolyte 80 µL of 1 M LiTFSI in TEGDME:DIOX 1:1 (by volume) was used. The separator consisted of four layers of disk-shaped Freudenberg 2190 with a diameter of 13 mm.

Scanning Electron Microscopy: A Carl Zeiss Auriga Modular Crossbeam workstation was utilized for the SEM characterization. The electron source was a Schottky field emission gun with a Gemini column. Images were taken at 3 kV accelerating voltage using an in lens secondary electron detector. The lens' aperture was 20 µm and the working distance 1.3 mm. The electron beam of the SEM did not show any modifications of the surface topology of lithium metal during exposure. The electrochemical cells were disassembled in an Ar filled glovebox (MBraun) and the lithium-metal anodes were washed with dimethoxyethane (Alfa Aesar) and dried in the antechamber. Afterward they were transported from the Ar glovebox to the SEM using an in-house-built sample transfer device that excludes any contact with oxygen and moisture from the atmosphere.

Atomic Force Microscopy: AFM measurements were performed with a 5500 Atomic Force Microscope (Agilent Technologies) using an arrow-shaped cantilever (Arrow CONT, NanoWorld). All images were recorded in the intermittent contact mode AC mode where the probe contacted the lithium-metal anode surface with a constant force. The experiments were performed under argon atmosphere and at room temperature.

Supporting Information

Supporting Information is available from the Wiley Online Library or from the author.

Acknowledgements

The authors acknowledge financial support from the European Commission through the Horizon 2020 framework program for research and innovation within the HELIS project under Grant Agreement no. 666221.

Conflict of Interest

The authors declare no conflict of interest.

Keywords

interfacial resistance, lithium anodes, lithium dissolution–deposition, native surface films, roll-press technique

Received: February 11, 2017
Revised: March 17, 2017
Published online: June 29, 2017

[1] R. Wagner, N. Preschitschek, S. Passerini, J. Leker, M. Winter, *J. Appl. Electrochem.* **2013**, *43*, 481.
[2] Y. Nishi, presented at 1996 Symp. on VLSI Circuits, 1996. Digest of Technical Papers, June **1996**.
[3] J. O. Besenhard, M. Winter, *Pure Appl. Chem.* **1998**, *70*, 603.
[4] Y. Nishi, *Chem. Rec.* **2001**, *1*, 406.
[5] M. Winter, J. O. Besenhard, M. E. Spahr, P. Novák, *Adv. Mater.* **1998**, *10*, 725.
[6] M. Winter, J. O. Besenhard, *Handbook of Battery Materials*, Wiley-VCH Verlag GmbH, Weinheim, Germany **2007**, p. 383.
[7] P. Bieker, M. Winter, *Chem. Unserer Zeit* **2016**, *50*, 172.
[8] J.-M. Tarascon, *Nat. Chem.* **2010**, *2*, 510.
[9] H. Kim, G. Jeong, Y.-U. Kim, J.-H. Kim, C.-M. Park, H.-J. Sohn, *Chem. Soc. Rev.* **2013**, *42*, 9011.
[10] W. Xu, J. Wang, F. Ding, X. Chen, E. Nasybulin, Y. Zhang, J.-G. Zhang, *Energy Environ. Sci.* **2014**, *7*, 513.
[11] R. G. Cao, W. Xu, D. P. Lv, J. Xiao, J. G. Zhang, *Adv. Energy Mater.* **2015**, *5*, 1402273.
[12] W. T. Gu, O. Borodin, B. Zdyrko, H. T. Lin, H. Kim, N. Nitta, J. X. Huang, A. Magasinski, Z. Milicev, G. Berdichevsky, G. Yushin, *Adv. Funct. Mater.* **2016**, *26*, 1507.
[13] M. Winter, J. O. Besenhard, *Chem. Unserer Zeit* **1999**, *33*, 252.
[14] R. W. Schmitz, P. Murmann, R. Schmitz, R. Müller, L. Krämer, J. Kasnatscheew, P. Isken, P. Niehoff, S. Nowak, G.-V. Röschenthaler, N. Ignatiev, P. Sartori, S. Passerini, M. Kunze, A. Lex-Balducci, C. Schreiner, I. Cekic-Laskovic, M. Winter, *Prog. Solid State Chem.* **2014**, *42*, 65.
[15] M. Winter, *Z. Phys. Chem.* **2009**, *223*, 1395.
[16] H. Schranzhofer, J. Bugajski, H. J. Santner, C. Korepp, K. C. Möller, J. O. Besenhard, M. Winter, W. Sitte, *J. Power Sources* **2006**, *153*, 391.
[17] J. Heine, P. Hilbig, X. Qi, P. Niehoff, M. Winter, P. Bieker, *J. Electrochem. Soc.* **2015**, *162*, A1094.
[18] X.-B. Cheng, R. Zhang, C.-Z. Zhao, F. Wei, J.-G. Zhang, Q. Zhang, *Adv. Sci.* **2016**, *3*, 1500213.
[19] H. T. T. Le, D. T. Ngo, V. C. Ho, G. Z. Cao, C. N. Park, C. J. Park, *J. Mater. Chem. A* **2016**, *4*, 11124.
[20] K. J. Harry, D. T. Hallinan, D. Y. Parkinson, A. A. MacDowell, N. P. Balsara, *Nat. Mater.* **2014**, *13*, 69.
[21] D. S. Eastwood, P. M. Bayley, H. J. Chang, O. O. Taiwo, J. Vila-Comamala, D. J. L. Brett, C. Rau, P. J. Withers, P. R. Shearing, C. P. Grey, P. D. Lee, *Chem. Commun.* **2015**, *51*, 266.
[22] G. Bieker, M. Winter, P. Bieker, *Phys. Chem. Chem. Phys.* **2015**, *17*, 8670.
[23] D. Lisbona, T. Snee, *Process Saf. Environ.* **2011**, *89*, 434.
[24] J. Heine, S. Krüger, C. Hartnig, U. Wietelmann, M. Winter, P. Bieker, *Adv. Energy Mater.* **2013**, *4*, 1.
[25] J. Heine, U. Rodehorst, X. Qi, J. P. Badillo, C. Hartnig, U. Wietelmann, M. Winter, P. Bieker, *Electrochim. Acta* **2014**, *138*, 288.
[26] A. Zhamu, G. Chen, C. Liu, D. Neff, Q. Fang, Z. Yu, W. Xiong, Y. Wang, X. Wang, B. Z. Jang, *Energy Environ. Sci.* **2012**, *5*, 5701.
[27] M.-H. Ryou, Y. M. Lee, Y. Lee, M. Winter, P. Bieker, *Adv. Funct. Mater.* **2015**, *25*, 834.
[28] J. Park, J. Jeong, Y. Lee, M. Oh, M.-H. Ryou, Y. M. Lee, *Adv. Mater. Interfaces* **2016**, *3*, 1600140.
[29] T. Schedlbauer, S. Krüger, R. Schmitz, R. W. Schmitz, C. Schreiner, H. J. Gores, S. Passerini, M. Winter, *Electrochim. Acta* **2013**, *92*, 102.
[30] P. Murmann, M. Börner, I. Cekic-Laskovic, M. Winter, *J. Appl. Electrochem.* **2016**, *46*, 339.
[31] X.-Q. Zhang, X.-B. Cheng, X. Chen, C. Yan, Q. Zhang, *Adv. Funct. Mater.* **2017**, *27*, 1605989.
[32] J.-i. Yamaki, S.-i. Tobishima, K. Hayashi, S. Keiichi, Y. Nemoto, M. Arakawa, *J. Power Sources* **1998**, *74*, 219.
[33] R. Schmitz, R. Müller, S. Krüger, R. W. Schmitz, S. Nowak, S. Passerini, M. Winter, C. Schreiner, *J. Power Sources* **2012**, *217*, 98.
[34] K. Kanamura, in *Encyclopedia of Electrochemical Power Sources* (Ed: J. Garche), Elsevier, Amsterdam **2009**, p. 27.
[35] M.-H. Ryou, Y. M. Lee, Y. Lee, M. Winter, P. Bieker, *Adv. Funct. Mater.* **2015**, *25*, 834.
[36] G. Eichkorn, H. Fischer, H. R. Mache, *Ber. Bunsenges. Phys. Chem.* **1971**, *75*, 482.
[37] L. Gireaud, S. Grugeon, S. Laruelle, B. Yrieix, J. M. Tarascon, *Electrochem. Commun.* **2006**, *8*, 1639.
[38] T. Fujieda, N. Yamamoto, K. Saito, T. Ishibashi, M. Honjo, S. Koike, N. Wakabayashi, S. Higuchi, *J. Power Sources* **1994**, *52*, 197.
[39] N.-W. Li, Y.-X. Yin, C.-P. Yang, Y.-G. Guo, *Adv. Mater.* **2016**, *28*, 1853.
[40] F. Marchioni, K. Star, E. Menke, T. Buffeteau, L. Servant, B. Dunn, F. Wudl, *Langmuir* **2007**, *23*, 11597.
[41] D. Lin, Y. Liu, Z. Liang, H.-W. Lee, J. Sun, H. Wang, K. Yan, J. Xie, Y. Cui, *Nat. Nanoechnol.* **2016**, *11*, 626.
[42] A. Budi, A. Basile, G. Opletal, A. F. Hollenkamp, A. S. Best, R. J. Rees, A. I. Bhatt, A. P. O'Mullane, S. P. Russo, *J. Phys. Chem. C* **2012**, *116*, 19789.
[43] A. I. Bhatt, P. Kao, A. S. Best, A. F. Hollenkamp, *J. Electrochem. Soc.* **2013**, *160*, A1171.
[44] M. R. Shoar Abouzari, F. Berkemeier, G. Schmitz, D. Wilmer, *Solid State Ionics* **2009**, *180*, 922.
[45] K. N. Wood, E. Kazyak, A. F. Chadwick, K.-H. Chen, J.-G. Zhang, K. Thornton, N. P. Dasgupta, *ACS Cent. Sci.* **2016**, *2*, 790.
[46] Y. Lu, Z. Tu, L. A. Archer, *Nat. Mater.* **2014**, *13*, 961.
[47] Q.-C. Liu, J.-J. Xu, S. Yuan, Z.-W. Chang, D. Xu, Y.-B. Yin, L. Li, H.-X. Zhong, Y.-S. Jiang, J.-M. Yan, X.-B. Zhang, *Adv. Mater.* **2015**, *27*, 5241.